Nonlinear Photocurrent Responses in Janus WSSe Monolayer

Meng Chen(陈盟)[1†], Sheng-Bin Yu(余盛斌)[2,3†], Dong Zhang(张东)[2,3], and Jun Li(李俊)[1*]

[1] *Department of Physics, Semiconductor Photonics Research Center, Xiamen University, Xiamen 361005, China*
[2] *SKLSM, Institute of Semiconductors, Chinese Academy of Sciences, Beijing 100083, China*
[3] *College of Materials Science and Opto-Electronic Technology, University of Chinese Academy of Sciences, Beijing 100049, China*

(Received 30 April 2023; accepted manuscript online 5 July 2023)

Janus WSSe monolayer is a novel two-dimensional (2D) material that breaks the out-of-plane mirror symmetry and has a large built-in electric field. These features lead to sizable Rashba spin-orbit coupling and enhanced nonlinear optical properties, making it a promising material platform for various spintronic and optoelectronic device applications. In recent years, nonlinear photocurrent responses such as shift and injection currents were found to be closely related to the quantum geometry and Berry curvature of materials, indicating that these responses can serve as powerful tools for probing the novel quantum properties of materials. In this work, we investigate the second-order nonlinear photocurrent responses in a Janus WSSe monolayer theoretically based on first-principles calculations and the Wannier interpolation method. It is demonstrated that the Janus WSSe monolayer exhibits significant out-of-plane nonlinear photocurrent coefficients, which is distinct from the non-Janus structures. Our results also suggest that the second-order nonlinear photocurrent response in the Janus WSSe monolayer can be effectively tuned by biaxial strain or an external electric field. Thus, the Janus WSSe monolayer offers a unique opportunity for both exploring nonlinear optical phenomena and realizing flexible 2D optoelectronic nanodevices.

DOI: 10.1088/0256-307X/40/8/087201

The successful fabrication of monolayer graphene in 2004[1] has led to the continuous growth of the field of two-dimensional (2D) materials. Their ultra-thin dimensions and excellent physical properties have attracted extensive attention from both fundamental research and device applications.[2–5] Among the emerging 2D materials, the transition metal dichalcogenides (TMDCs) exhibit various unique properties, such as tunable semiconductor bandgap, strong spin-orbit coupling (SOC), spin-valley locking, and valley-contrasting properties, making them potential candidates for next-generation nanoelectronic, optoelectronic and valleytronic devices.[6–9]

Recently, a new class of 2D materials known as Janus TMDCs has been successfully synthesized in experiments, and there are examples including Janus MoSSe,[10,11] Janus WSSe,[12,13] and other Janus structures.[14,15] These materials are formed by substituting one sublayer of chalcogen atoms with another element, and their unique structure breaks the out-of-plane mirror symmetry and facilitates charge transfer, which produces an intrinsic out-of-plane electric dipole moment and a large built-in electric field. As a result, the 2D Janus TMDCs were predicted to host several nontrivial properties, such as sizable Rashba SOC and spin Hall effect,[16,17] strong piezoelectric response,[18] long exciton lifetimes,[19] enhanced interlayer coupling,[20] large current-induced spin polarization,[21] and nonlinear planar Hall effect.[22] In particular, symmetry breaking in Janus TMDCs has a significant impact on nonlinear optical properties, such as out-of-plane second harmonic generation,[23] bulk photovoltaic effect,[24–26] nonlinear anomalous Hall effect,[27] and angular dependence of the second-order nonlinear optical response.[28] These phenomena are closely related to the quantum geometry and Berry curvature of the material, and provide important means for exploring the novel quantum properties of the materials.[29–32] Therefore, the Janus TMDCs monolayers could be suitable candidates in 2D nonlinear optical applications.

Furthermore, it has been found that the linear optical properties of Janus TMDCs depend strongly on the intrinsic electric dipole moment of the material and can be tuned by strain and external electric field.[16,32] For instance, the light absorption intensity of Janus Ga_2SSe, PtSSe, and Al_2SSe monolayers can be significantly enhanced by tensile strain.[33–35] However, the influences of strain and external electric field on the nonlinear photocurrent responses of Janus TMDCs monolayers have not yet been explored. In this Letter, we investigate the second-order nonlinear photocurrent response of the Janus WSSe monolayer by combining first-principles calculation and the Wannier interpolation method. We analyze the characteristics of the injection and shift current coefficients, and show that the second-order nonlinear photocurrent response can be tuned by biaxial strain or external electric field. Our calculation results may provide guidance for potential applications in optoelectronics, valleytronics, and spintronics.

†These authors contributed equally to this work.
*Corresponding author. Email: lijun@xmu.edu.cn
© 2023 Chinese Physical Society and IOP Publishing Ltd

Calculation Methods. We carry out first-principles calculations based on the density functional theory (DFT)[36,37] using the Vienna *ab initio* simulation package (VASP) code[38,39] with the projector-augmented wave pseudopotential method,[40] and the Perdew–Burke–Ernzerhof exchange-correlation functional.[41] We consider a free-standing Janus WSSe monolayer placed in the x–y plane and add a vacuum layer of 20 Å along the z direction to avoid unphysical interactions due to the periodic boundary condition. An out-of-plane dipole correction is introduced in our calculations due to the presence of the intrinsic electric dipole moment in the Janus WSSe monolayer.[42] During the crystal structure relaxation procedure, we fix the c-axis of the lattice and fully relax the structures until the maximum force on each atom is less than 0.001 eV/Å. A plane wave cutoff energy of 600 eV is used and the convergence criterion for the total energy is set to 10^{-8} eV. For the in-plane biaxial strain in the Janus WSSe monolayer, the strain ε is defined as $\varepsilon = (a-a_0)/a_0$, where a_0 is the equilibrium lattice constant, and a is the lattice constant under strain. Compressive strain corresponds to $\varepsilon < 0$, and tensile strain corresponds to $\varepsilon > 0$. For the external electric field, the direction of the positive electric field E is defined along the z direction.

After performing first-principles calculations, we can obtain the electronic structure data of the Janus WSSe monolayer on a $21 \times 21 \times 1$ Monkhorst–Pack $\boldsymbol{q}$-grid, i.e., involving the eigenenergies $[E_n(\boldsymbol{q})]$, orbital projections of wave functions ($\langle\psi_{m\boldsymbol{q}}|g_n\rangle$) and overlaps between Bloch orbitals at neighboring $\boldsymbol{q}$-points ($\langle u_{m\boldsymbol{q}}|u_{n,\boldsymbol{q}+\boldsymbol{b}}\rangle$). We use the Wannier90 package to construct maximally localized Wannier functions (MLWFs) from these data.[43,44] In the Wannier gauge, the matrix elements of Hamiltonian operator $\hat{\boldsymbol{H}}$ are defined as $H^{(\mathrm{W})}_{nm}(\boldsymbol{q}) = \langle u^{(\mathrm{W})}_{n\boldsymbol{q}}|\hat{\boldsymbol{H}}|u^{(\mathrm{W})}_{m\boldsymbol{q}}\rangle = [V^{+}(\boldsymbol{q})H^{0}(\boldsymbol{q})V(\boldsymbol{q})]_{nm}$, where $V(\boldsymbol{q})$ is a unitary matrix that minimize the spreads of the MLWFs, and $\boldsymbol{q}$ represents a Monkhorst–Pack grid point. In order to reconstruct the continuous signal $H^{(\mathrm{W})}_{nm}(\boldsymbol{q})$ at any $\boldsymbol{k}$ point, we first Fourier transform the Hamiltonian matrix elements from reciprocal space to real space. This generates the real-space Wannier Hamiltonian matrix elements $H^{(\mathrm{W})}_{nm}(\boldsymbol{R}) \equiv \langle 0|\hat{\boldsymbol{H}}|\boldsymbol{R}\rangle = \frac{1}{N}\sum_{\boldsymbol{q}=\boldsymbol{q}_1,\ldots,\boldsymbol{q}_N} e^{-i\boldsymbol{q}\cdot\boldsymbol{R}} H^{(\mathrm{W})}_{nm}(\boldsymbol{q})$, where N is the total number of Monkhorst–Pack grid points. Thanks to the real-space localization of the Wannier functions, the matrix elements $H^{(\mathrm{W})}_{nm}(\boldsymbol{R})$ die out when the distances between the Wannier centers exceed a critical value. This allows us to cut off $H^{(\mathrm{W})}_{nm}(\boldsymbol{R})$ at a finite $\boldsymbol{R}_m$. Then, we can safely perform an inverse Fourier transform back to reciprocal space to construct the Wannier-interpolation Hamiltonian $H^{(\mathrm{W})}_{nm}(\boldsymbol{k}) = \sum_{|\boldsymbol{R}|\le\boldsymbol{R}_m} e^{i\boldsymbol{k}\cdot\boldsymbol{R}} H^{(\mathrm{W})}_{nm}(\boldsymbol{R})$, where $\boldsymbol{k}$ represents an arbitrary interpolation grid point. Finally, by diagonalizing $H^{(\mathrm{W})}_{nm}(\boldsymbol{k})$, we can attain the eigenenergies, eigenstates, velocity matrix elements and Berry connections on a finer interpolation grid ($400 \times 400 \times 1$). This enables efficient calculations of Brillouin-zone integration when computing the nonlinear photocurrent response coefficients.

In this work, we focus on the second-order DC photocurrent responses of monolayer Janus WSSe. They can be characterized by the injection current generation rate tensor $\eta^{\mathrm{injection}}_{\mu,\alpha\beta}$ and the shift current susceptibility tensor $\sigma^{\mathrm{shift}}_{\alpha,\beta\beta}$, respectively.[45] Under the independent-particle approximation, the injection current generation rate susceptibility tensor is given by[25,45]

$$\eta^{\mathrm{injection}}_{\mu,\alpha\beta}(0;\omega,-\omega) = \frac{i\pi e^3}{2\hbar^2}\int [d\boldsymbol{k}] \sum_{nm} f_{nm}\Delta^{\alpha,\beta}_{nm}\Omega^{\alpha,\beta}_{mn}(\boldsymbol{k})\delta(\omega_{mn}-\omega), \quad (1)$$

where $[dk] \equiv \frac{d\boldsymbol{k}}{(2\pi)^d}$ and d is the number of dimensions; $f_{nm} \equiv f(\epsilon_n) - f(\epsilon_m)$ is the difference of Fermi–Dirac distributions; $\Omega^{\alpha,\beta}_{mn}(\boldsymbol{k}) \equiv i[r^{\alpha}_{mn}, r^{\beta}_{nm}] = -i[r^{\beta}_{mn}, r^{\alpha}_{nm}]$ is the band-resolved Berry curvature between bands m and n, with $r_{nm} = i\langle n|\nabla_{\boldsymbol{k}}|m\rangle$ representing the interband Berry connection. Similarly, the intraband Berry connection can be expressed as $\mathcal{A}_n(\boldsymbol{k}) = i\langle n|\nabla_{\boldsymbol{k}}|n\rangle$. Here, $\hbar\Delta^{\alpha,\beta}_{mn} = v^{\alpha}_{mm} - v^{\beta}_{nn}$ is the group velocity difference between bands m and n. In our calculations, $\delta(\omega_{mn}-\omega)$ has been replaced by the Lorentzian function $\gamma/\pi[(\omega_{mn}-\omega)^2+\gamma^2]$, where γ (set to 0.02 eV) is the broadening factor, and $\int[d\boldsymbol{k}]\sum_{nm}\delta(\omega_{mn}-\omega)$ defines the joint density of states. Therefrom, the shift current susceptibility tensor is[25,45]

$$\sigma^{\mathrm{shift}}_{\alpha,\beta\beta}(0;\omega,-\omega) = -\frac{\pi e^3}{2\hbar^2}\int [d\boldsymbol{k}] \sum_{nm} f_{nm} R^{\alpha,\beta}_{nm}(\boldsymbol{k}) r^{\beta}_{nm} r^{\beta}_{mn}\delta(\omega_{mn}-\omega), \quad (2)$$

where $r^{\beta}_{nm}r^{\beta}_{mn}$ is the transition matrix element. $R^{\alpha,\beta}_{nm}(\boldsymbol{k}) = -\frac{\partial^{\beta}\phi_{nm}(\boldsymbol{k})}{\partial k^{\alpha}} + \mathcal{A}^{\alpha}_{n}(\boldsymbol{k}) - \mathcal{A}^{\alpha}_{m}(\boldsymbol{k})$ is the shift vector, with $\phi_{nm}(\boldsymbol{k})$ being the phase factor of the interband Berry connection $r_{nm}(\boldsymbol{k}) = |r_{nm}(\boldsymbol{k})|e^{i\phi_{nm}(\boldsymbol{k})}$. All the above physical parameters can be obtained by applying the Wannier interpolation method.[46,47]

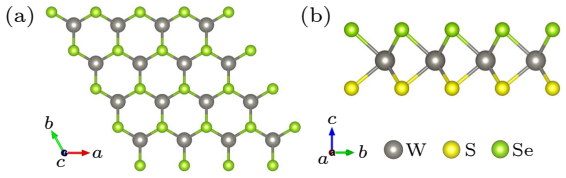

Fig. 1. Schematic of the Janus WSSe monolayer structure: (a) top view, (b) side view.

Results and Discussion. The crystal structure of the Janus WSSe monolayer is shown in Fig. 1. The equilibrium in-plane lattice constant is 3.25 Å after relaxing, and the bond lengths of W–S and W–Se are 2.43 Å and 2.54 Å, respectively. Compared to the WS_2 and WSe_2 monolayers, the point group of the Janus WSSe monolayer is reduced from D_{3h} to C_{3v} due to breaking of the out-of-plane mirror symmetry. This leads to charge transfer between the S and Se sublayers in the Janus WSSe monolayer and the appearance of out-of-plane electric polarization, which strongly affects both the electronic structure and optical response of Janus WSSe. As shown in Fig. 2(a), there is an energy difference of about 0.7 eV between the S and Se layers, which indicates their different work functions. We employ Bader charge analysis to calculate the charge distribution between the W atom and the S/Se atom and find that the S atom gains a charge of $0.76e$, while the Se atom only gains a charge of $0.73e$. Therefore, this asymmetric charge distribution creates a net out-of-plane electric

dipole moment pointing from Se to S (−0.17 D) and induces an intrinsic built-in electric field, which agree with those reported Ref. [48].

The band structure of the Janus WSSe monolayer (with SOC) is depicted in Fig. 2(b). It shows that the Janus WSSe monolayer is a semiconductor with a direct bandgap of 1.418 eV. Both the conduction-band minimum (CBM) and the valence-band maximum (VBM) are located at the K point of the Brillouin zone, consistent with the previous reports.[49] Compared to their parent pristine materials, the electronic properties of the Janus structure are significantly altered. For example, the bandgap of WS_2 is 1.552 eV, while that of WSSe is 1.418 eV, and that of WSe_2 is 1.257 eV. To construct MLWFs, the d orbitals of the W atom and the s and p orbitals of S/Se atoms are selected as the initial projected orbitals because they are the main orbital components near the Fermi level.[?,51] To obtain high-quality MLWFs, appropriate energy windows must be selected to fit the band structures obtained by first-principles calculations. As manifested in Fig. 2(b), the band structure calculated by diagonalizing $H_{nm}^{(\mathrm{W})}(\boldsymbol{k})$ is consistent with the result obtained from the first-principles calculation, which indicates that the Wannier-interpolation Hamiltonian is well constructed.

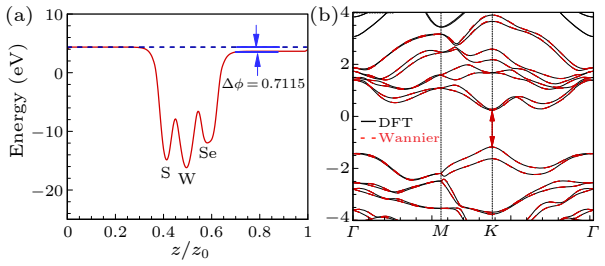

Fig. 2. (a) The average electrostatic potential of the Janus WSSe monolayer. (b) The band structures of the Janus WSSe monolayer, where black- and red-colored lines are the DFT and Wannier-interpolation calculation results, respectively.

Using the obtained Wannier-interpolation Hamiltonian $H_{nm}^{(\mathrm{W})}(\boldsymbol{k})$, we developed a parallel computing program that can be used to efficiently calculate the injection current generation rate and shift current susceptibility tensors. According to Eq. (1), the injection current generation rate $\eta_{\mu,\alpha\beta}^{\mathrm{injection}}$ is a third-order tensor. Due to the C_{3v} symmetry of the Janus WSSe monolayer, only 4 of the 27 tensor components are non-zero and equivalent: $\eta_{xxz} = \eta_{yzy} = -\eta_{xzx} = -\eta_{yyz}$. Thus, there is only one independent injection current component for the Janus WSSe monolayer. As presented in Fig. 3(a), in contrast to WS_2 and WSe_2 monolayers, the Janus WSSe monolayer exhibits circularly polarized photocurrent responses that are absent in non-Janus structures. According to Eq. (2), the shift current susceptibility tensor $\sigma_{\mu,\alpha\beta}^{\mathrm{shift}}$ is also a third-order tensor. Of the 27 tensor components, the $\sigma_{\mu,\alpha\beta}^{\mathrm{shift}}$ has 11 non-zero tensor components with 4 independent components: σ_{zzz}, $\sigma_{zxx} = \sigma_{zyy}$, $\sigma_{yyy} = -\sigma_{xxy} = -\sigma_{yxx} = -\sigma_{xyx}$, $\sigma_{xxz} = \sigma_{xzx} = \sigma_{yyz} = \sigma_{yzy}$. Compared to WS_2 and WSe_2 monolayers, the breaking of the out-of-plane mirror symmetry in the Janus WSSe monolayer adds 3 additional non-zero tensor components, all related to the z direction. Interestingly, σ_{yyy} is the strongest shift current response, followed by σ_{xxz}. The in-plane tensor component σ_{yyy} has its peak response in the range of 3–4 eV. The smallest tensor component σ_{zzz} is more active for photons with energies above 4 eV. Therefore, the absence of mirror symmetry in the Janus WSSe monolayer generates a non-zero component of the injection current, while it vanishes in the parent pristine materials. Furthermore, breaking the mirror inversion symmetry in the Janus WSSe monolayer increases the non-zero tensor components in the shift current, while WS_2 and WSe_2 monolayers have only one non-zero component.

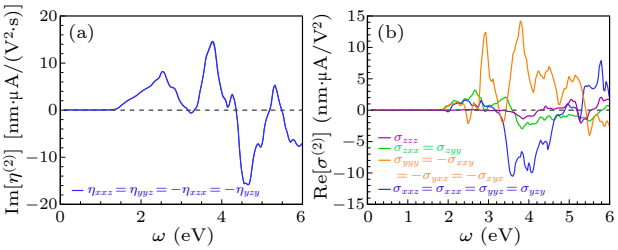

Fig. 3. (a) Injection current generation rate susceptibility tensor $\eta_{\mu,\alpha\beta}^{\mathrm{injection}}$ and (b) shift current susceptibility tensor $\sigma_{\mu,\alpha\beta}^{\mathrm{shift}}$ of the Janus WSSe monolayer.

Strain engineering is an effective approach to tune the electronic structure of 2D materials. Figure 4(a) exhibits the band structure of the Janus WSSe monolayer under different biaxial strains. Applying a compressive strain keeps the VBM at the K point of the Brillouin zone, but shifts the CBM from the K point to the Γ point, resulting in an indirect band semiconductor. When a tensile strain is applied, the VBM moves from the K point to the Γ point in the entire strain range, and also produces an indirect band gap semiconductor. However, increasing the tensile strain significantly reduces the bandgap of the Janus WSSe monolayer and shows an approximately linear dependence.

Applying an external electric field offers another way to tune the band structure of 2D materials. The response of a material to an external electric field E depends on the magnitude of the electric polarization, which is related to the occupation of electrons in the valence bands. Due to the giant built-in electric field in the Janus WSSe monolayer, an external electric field can only induce relatively low electric polarization. As a result, the bandgap of the Janus WSSe monolayer changes only slightly under an external electric field E. Figure 4(b) shows the band structure of the Janus WSSe monolayer under an external electric field ranging from −0.5 V/Å to 0.5 V/Å. The higher external electric field increases the Coulomb interaction between the electric field and the electric polarization of valence electrons, resulting in a nearly constant rate of bandgap change in the Janus WSSe monolayer.

Since strain effectively modifies the electronic band structure of the Janus WSSe monolayer, its optical properties can be tuned simultaneously. Figure 5(a) displays the injection current generation rate susceptibility $\eta_{\mu,\alpha\beta}^{\mathrm{injection}}$ of the Janus WSSe monolayer under biaxial strain from −5%

to 5%. Because biaxial strain does not change the structure symmetry of the Janus WSSe monolayer, the nonzero tensor components still satisfy $\eta_{xxz} = \eta_{yzy} = -\eta_{xzx} = -\eta_{yyz}$. The injection current response varies significantly under biaxial strain. Tensile strain effectively reduces it, while compressive strain enhances it accordingly. The intensity of the main peak changes drastically under biaxial strain, especially under compressive strain where it increases. However, the main peak position remains stable. As shown in Fig. 5(b), an external electric field ranging from $-0.5\,\mathrm{V/Å}$ to $0.5\,\mathrm{V/Å}$ has relatively little effect on the injection current response of the Janus WSSe monolayer. A positive electric field slightly enhances the injection current response while a negative electric field reduces it. The magnitude of the electric field is proportional to $\eta^{\mathrm{injection}}_{\mu,\alpha\beta}$. When the incident photon energy is in the range of 2.5–3.5 eV or 5–6 eV, the electric field has a more significant effect on the injection current response of the Janus WSSe monolayer.

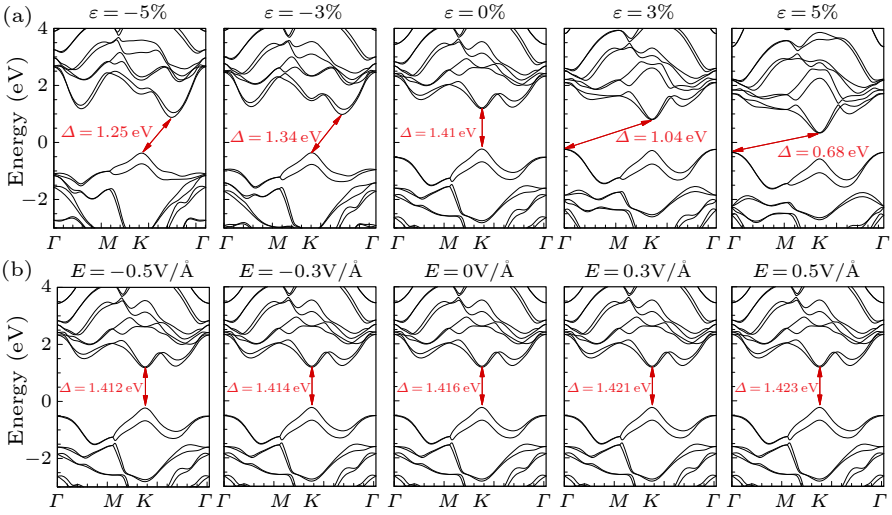

Fig. 4. Band structure of the Janus WSSe monolayer (a) under biaxial strain and (b) in an external electric field.

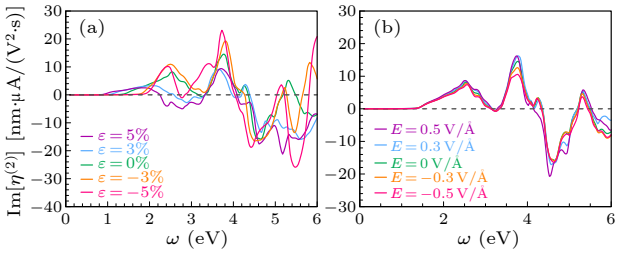

Fig. 5. Injection current generation rate susceptibility tensor $\eta^{\mathrm{injection}}_{\mu,\alpha\beta}$ of the Janus WSSe monolayer (a) under biaxial strain and (b) in applied electric field.

Biaxial strain also significantly affects the shift current susceptibility tensor $\sigma^{\mathrm{shift}}_{\mu,\alpha\beta}$ of the Janus WSSe monolayer, as presented in Fig. 6. Since the symmetry of the Janus WSSe monolayer remains C_{3v} under biaxial strain, the total number of nonzero independent tensor components remains unchanged. Contrary to the injection current, the shift current response strengthens under tensile strain, while it weakens significantly under compressive strain. The intensity of the main peak varies dramatically under the biaxial strain from −5% to 5%, especially under tensile strain where it increases and the main peak position shifts as well. Tensile strain makes $\sigma^{\mathrm{shift}}_{\mu,\alpha\beta}$ of the Janus WSSe monolayer reach its highest value at a low incident photon energy. However, under compressive strain, a larger incident photon energy is required to reach the maximum value. Notably, tensile strain can enhance the peak value of the shift current response.

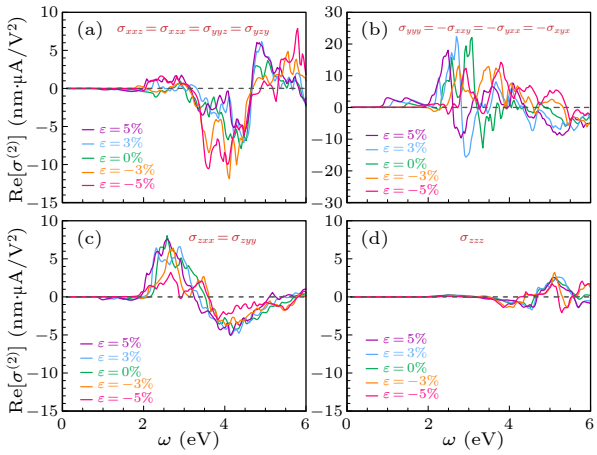

Fig. 6. Shift current susceptibility tensor $\sigma^{\mathrm{shift}}_{\mu,\alpha\beta}$ of the Janus WSSe monolayer under biaxial strain. Nonzero independent tensor components includes (a) $\sigma_{xxz} = \sigma_{xzx} = \sigma_{yyz} = \sigma_{yzy}$, (b) $\sigma_{yyy} = -\sigma_{xxy} = -\sigma_{yxx} = -\sigma_{xyx}$, (c) $\sigma_{zxx} = \sigma_{zyy}$, and (d) σ_{zzz}.

Finally, we discuss the influence of external electric field on the shift current susceptibility tensor $\sigma^{\mathrm{shift}}_{\mu,\alpha\beta}$ in the Janus WSSe monolayer. As shown in Fig. 7, the effect of an external electric field ranging from $-0.5\,\mathrm{V/Å}$ to $0.5\,\mathrm{V/Å}$ on the shift current response is similar to that of the injection current response in the Janus WSSe monolayer. A positive electric field slightly enhances the shift current response while a negative one reduces it. The magnitude of the electric field is proportional to $\eta^{\mathrm{injection}}_{\mu,\alpha\beta}$. When the

incident photon energy is in the range of 2.5–3.5 eV or 5–6 eV, the electric field has a greater impact on the shift current response of the Janus WSSe monolayer. This observation aligns with the principle that an external electric field alters the injection current. Additionally, the out-of-plane shift current susceptibility tensor components are more sensitive to the electric field than their in-plane counterparts due to changes in the intrinsic electric dipole moment of the Janus WSSe monolayer.

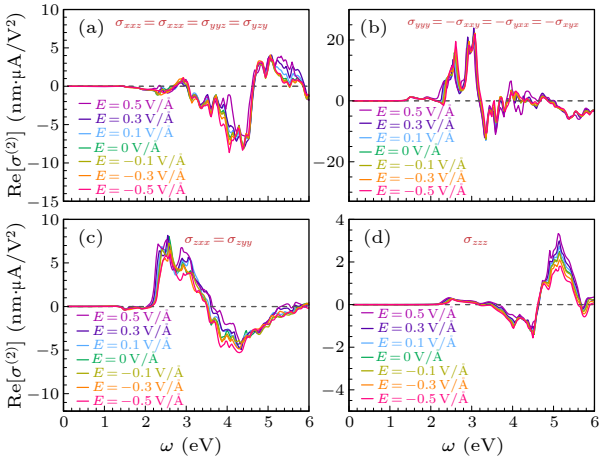

Fig. 7. Shift current susceptibility tensor $\sigma^{\mathrm{shift}}_{\mu,\alpha\beta}$ of the Janus WSSe monolayer under external electric field from −0.5 V/Å to 0.5 V/Å. Nonzero independent tensor components includes (a) $\sigma_{xxz} = \sigma_{xzx} = \sigma_{yyz} = \sigma_{yzy}$, (b) $\sigma_{yyy} = -\sigma_{xxy} = -\sigma_{yxx} = -\sigma_{xyx}$, (c) $\sigma_{zxx} = \sigma_{zyy}$, and (d) σ_{zzz}.

In summary, using first-principles calculations and the Wannier interpolation method, we have theoretically investigated the electronic structures and second-order nonlinear photocurrent responses of a Janus WSSe monolayer. The bandgap of the Janus WSSe monolayer is 1.418 eV which lies between WS_2 and WSe_2 monolayers. The breaking of the out-of-plane mirror symmetry creates an electric dipole moment of 0.173 D in the Janus WSSe monolayer, pointing from the Se sublayer to the S sublayer. The Janus WSSe monolayer exhibits strong out-of-plane second-order nonlinear photocurrent responses that are absent in non-Janus structures. This provides a method for experimentally identifying Janus TMDCs monolayers and their parent pristine TMDCs monolayers. The second-order nonlinear photocurrent response of the Janus WSSe monolayer can be effectively modulated by biaxial strain or an external electric field. Both the shift and injection current responses vary significantly under biaxial strain, with the peak value of the injection current response remaining nearly unchanged while that of the shift current response shifts. The effect of an external electric field on the shift and injection current responses of the Janus WSSe monolayer is relatively weak. When the external electric field is between −0.5 and 0.5 V/Å, the magnitude of the nonlinear photocurrent susceptibility tensor is proportional to the external electric field and the influence of an external electric field under 0.5 V/Å is more significant. Additionally, due to the built-in electric field of the Janus WSSe monolayer, the effect of an external electric field on shift current response along the z direction is larger. These results suggest that the Janus WSSe monolayer offers a unique opportunity for exploring nonlinear optical phenomena and has great potential in optoelectronic applications.

Acknowledgements. This work was supported by the Natural Science Foundation of Fujian Province of China (Grant No. 2020J01008), and the National Natural Science Foundation of China (Grant No. 12174382).

References

[1] Novoselov K S, Geim A K, Morozov S V, Jiang D, Zhang Y, Dubonos S V, Grigorieva I V, and Firsov A A 2004 *Science* **306** 666
[2] Geim A K and Grigorieva I V 2013 *Nature* **499** 419
[3] Castellanos-Gomez A 2016 *Nat. Photon.* **10** 202
[4] Xia F N, Wang H, Xiao D, Dubey M, and Ramasubramaniam A 2014 *Nat. Photon.* **8** 899
[5] Lin X Y, Yang W, Wang K L, and Zhao W S 2019 *Nat. Electron.* **2** 274
[6] Manzeli S, Ovchinnikov D, Pasquier D, Yazyev O V, and Kis A 2017 *Nat. Rev. Mater.* **2** 17033
[7] Xu X D, Yao W, Xiao D, and Heinz T F 2014 *Nat. Phys.* **10** 343
[8] Mak K F and Shan J 2016 *Nat. Photon.* **10** 216
[9] Chen Y D, Huang Y W, Lou W K, Cai Y Y, and Chang K 2020 *Phys. Rev. B* **102** 165413
[10] Lu A Y, Zhu H, Xiao J, Chuu C P, Han Y, Chiu M H, Cheng C C, Yang C W, Wei K H, Yang Y, Wang Y, Sokaras D, Nordlund D, Yang P, Muller D A, Chou M Y, Zhang X, and Li L J 2017 *Nat. Nanotechnol.* **12** 744
[11] Zhang J, Jia S, Kholmanov I, Dong L, Er D, Chen W, Guo H, Jin Z, Shenoy V B, Shi L, and Lou J 2017 *ACS Nano* **11** 8192
[12] Lin Y C, Liu C, Yu Y, Zarkadoula E, Yoon M, Puretzky A A, Liang L, Kong X, Gu Y, Strasser A, Meyer H M, Lorenz M, Chisholm M F, Ivanov I N, Rouleau C M, Duscher G, Xiao K, and Geohegan D B 2020 *ACS Nano* **14** 3896
[13] Han Z C, Wei T Y, Xiao Q Y, Zhong X Y, Xiang D, and Liu T 2022 *Appl. Phys. Lett.* **120** 221901
[14] Trivedi D B, Turgut G, Qin Y, Sayyad M Y, Hajra D, Howell M, Liu L, Yang S, Patoary N H, Li H, Petrić M M, Meyer M, Kremser M, Barbone M, Soavi G, Stier A V, Müller K, Yang S, Esqueda I S, Zhuang H, Finley J J, and Tongay S 2020 *Adv. Mater.* **32** 2006320
[15] Qin Y, Sayyad M, Montblanch A R P, Feuer M S G, Dey D, Blei M, Sailus R, Kara D M, Shen Y, Yang S, Botana A S, Atature M, and Tongay S 2022 *Adv. Mater.* **34** 2106222
[16] Yao Q F, Cai J, Tong W Y, Gong S J, Wang J Q, Wan X, Duan C G, and Chu J H 2017 *Phys. Rev. B* **95** 165401
[17] Yu S B, Zhou M, Zhang D, and Chang K 2021 *Phys. Rev. B* **104** 075435
[18] Dong L, Lou J, and Shenoy V B 2017 *ACS Nano* **11** 8242
[19] Zheng T, Lin Y C, Yu Y L, Valencia-Acuna P, Puretzky A A, Torsi R, Liu C, Ivanov I N, Duscher G, Geohegan D B, Ni Z H, Xiao K, and Zhao H 2021 *Nano Lett.* **21** 931
[20] Zhang K X, Guo Y F, Ji Q Q, Lu A Y, Su C, Wang H, Puretzky A A, Geohegan D B, Qian X F, Fang S, Kaxiras E, Kong J, and Huang S X 2020 *J. Am. Chem. Soc.* **142** 17499
[21] Yu S B, Sun S H, Zhou M, Zhang D, and Chang K 2023 *Phys. Rev. B* **107** 125426
[22] Huang Y X, Feng X L, Wang H, Xiao C, and Yang S A 2023 *Phys. Rev. Lett.* **103** 126303
[23] Wei Y D, Xu X D, Wang S S, Li W Q, and Jiang Y Y 2019 *Phys. Chem. Chem. Phys.* **21** 21022
[24] Xu H W, Wang H, Zhou J, Guo Y F, Kong J, and Li J 2021 *npj Comput. Mater.* **7** 31
[25] Strasser A, Wang H, and Qian X F 2022 *Nano Lett.* **22** 4145
[26] Dai Z B and Rappe A M 2023 *Chem. Phys. Rev.* **4** 011303

[27] Karmakar S, Biswas R, and Saha-Dasgupta T 2023 *Phys. Rev. B* **107** 075403
[28] Pike N A and Pachter R J 2022 *J. Phys. Chem. C* **126** 16243
[29] Jürgens P, Liewehr B, Kruse B, Peltz C, Engel D, Husakou A, Witting T, Ivanov M, Vrakking M J J, Fennel T, and Mermillod-Blondin A 2020 *Nat. Phys.* **16** 1035
[30] Qian C, Yu C, Jiang S C, Zhang T, Gao J C, Shi S, Pi H Q, Weng H M, and Lu R F 2022 *Phys. Rev. X* **12** 021030
[31] Ma Q, Grushin A G, and Burch K S 2021 *Nat. Mater.* **20** 1601
[32] Yagmurcukardes M, Qin Y, Ozen S, Sayyad M, Peeters F M, Tongay S, and Sahin H 2020 *Appl. Phys. Rev.* **7** 011311
[33] Nguyen H T T, Vi V T T, Vu T V, Hieu N V, Lu D V, Rai D P, and Binh N T T 2020 *RSC Adv.* **10** 44785
[34] Vo D D, Vu T V, Al-Qaisi S, Tong H D, Le T S, Nguyen C V, Phuc H V, Luong H L, Jappor H R, Obeid M M, and Hieu N N 2020 *Superlattices Microstruct.* **147** 106683
[35] Nhan L C, Nguyen C Q, Hieu N V, Phuc H V, Nguyen C V, Hieu N N, Vu T V, and Nguyen H T T 2021 *Optik* **238** 166761
[36] Hohenberg P and Kohn W 1964 *Phys. Rev.* **136** B864
[37] Kohn W and Sham L J 1965 *Phys. Rev.* **140** A1133
[38] Kresse G and Hafner J 1994 *Phys. Rev. B* **49** 14251
[39] Kresse G and Furthmüller J 1996 *Phys. Rev. B* **54** 11169
[40] Blöchl P E 1994 *Phys. Rev. B* **50** 17953
[41] Perdew J P, Burke K, and Ernzerhof M 1996 *Phys. Rev. Lett.* **77** 3865
[42] Neugebauer J and Scheffler M 1992 *Phys. Rev. B* **46** 16067
[43] Marzari N, Mostofi A A, Yates J R, Souza I, and Vanderbilt D 2012 *Rev. Mod. Phys.* **84** 1419
[44] Pizzi G, Vitale V, Arita R, Blügel S, Freimuth F, Géranton G, Gibertini M, Gresch D, Johnson C, Koretsune T, Iba N A J, Lee H, Lihm J M, Marchand D, Marrazzo A, Mokrousov Y, Mustafa J I, Nohara Y, Nomura Y, Paulatto L, Poncé S, Ponweiser T, Qiao J, Thöle F, Tsirkin S S, Wierzbowska M, Marzari N, Vanderbilt D, Souza I, Mostofi A A, and Yates J R 2020 *J. Phys.: Condens Matter.* **32** 165902
[45] Sipe J E and Shkrebtii A I 2000 *Phys. Rev. B* **61** 5337
[46] Wang C, Liu X Y, Kang L, Gu B L, Xu Y, and Duan W H 2017 *Phys. Rev. B* **96** 115147
[47] Iba N A J, Tsirkin S S, and Souza I 2018 *Phys. Rev. B* **97** 245143
[48] Xia C X, Xiong W Q, Du J, Wang T X, Peng Y T, and Li J B 2018 *Phys. Rev. B* **98** 165424
[49] Zhou W Z, ChenJ Y, Yang Z X, Liu J W, and Ouyang F P 2019 *Phys. Rev. B* **99** 075160
[50] Marzari N and Vanderbilt D 1997 *Phys. Rev. B* **56** 12847
[51] Souza I, Marzari N, and Vanderbilt D 2001 *Phys. Rev. B* **65** 035109